Rock and Soil Mechanics

Volume 43 | Issue 2 Article 7

4-14-2022

Experimental study and numerical simulation on the migration and transformation mechanism of hexavalent chromium in contaminated site

Yong HE
School of Geosciences and Info-Physics, Central South University, Changsha, Hunan 410083, China

Guang HU
School of Geosciences and Info-Physics, Central South University, Changsha, Hunan 410083, China

Zhao ZHANG
School of Geosciences and Info-Physics, Central South University, Changsha, Hunan 410083, China

Wei LOU
Hunan HIKEE Environmental Technology Co., Ltd., Changsha, Hunan 410221, China

See next page for additional authors

Custom Citation

HE Yong, HU Guang, ZHANG Zhao, LOU Wei, ZOU Yan-hong, LI Xing, ZHANG Ke-neng, . Experimental study and numerical simulation on the migration and transformation mechanism of hexavalent chromium in contaminated site[J]. Rock and Soil Mechanics, 2022, 43(2): 528-538.

Experimental study and numerical simulation on the migration and transformation mechanism of hexavalent chromium in contaminated site

Authors

Yong HE, Guang HU, Zhao ZHANG, Wei LOU, Yan-hong ZOU, Xing LI, and Ke-neng ZHANG

Rock and Soil Mechanics 2022 43(2): 528−538 ISSN 1000−7598
https: //doi.org/10.16285/j.rsm.2021.6255 rocksoilmech.researchcommons.org/journal

Experimental study and numerical simulation on the migration and transformation mechanism of hexavalent chromium in contaminated site

HE Yong[1, 2], HU Guang[1, 2], ZHANG Zhao[1, 2], LOU Wei[3], ZOU Yan-hong[1, 2], LI Xing[3], ZHANG Ke-neng[1, 2]

1. Key Laboratory of Metallogenic Prediction of Nonferrous Metals and Geological Environment Monitoring, Ministry of Education, Central South University, Changsha, Hunan 410083, China

2. School of Geosciences and Info-Physics, Central South University, Changsha, Hunan 410083, China

3. Hunan HIKEE Environmental Technology Co., Ltd., Changsha, Hunan 410221, China

Abstract: With the rapid development of global industrialization, the pollution of hexavalent chromium (Cr(Ⅵ)) in soil and groundwater has become increasingly serious. Field investigation and laboratory tests were carried out for the soil polluted by the chromium slag of a ferroalloy plant. The adsorption, infiltration and dispersion experiments were conducted to study the adsorption characteristics and migration mechanism of Cr(Ⅵ) in silty clay. A three-dimensional kinetic mathematical model of Cr(Ⅵ) migration considering convection-dispersion-adsorption was established. The migration and distribution characteristics of Cr(Ⅵ) in groundwater with the pollution source located upstream or downstream of the contaminated site were obtained using the numerical approach. Meanwhile, the effects of dispersity (α) and distribution coefficient (K_d) on the spatial and temporal distribution of Cr(Ⅵ) were revealed. The experimental results show that the Langmuir isotherm model well fits the adsorption data of silty clay. The maximum adsorption capacity of silty clay for Cr(Ⅵ) was 466.6 mg/kg. The hydraulic conductivity of silty clay under the infiltration of distilled water and 160 mg/L Cr(Ⅵ) solution was 6.5×10^{-7}–6.7×10^{-7} cm/s, while it increased to 4.4×10^{-6} cm/s under infiltration of Cr(Ⅵ) solution with a concentration of 1 000 mg/L. The hydrodynamic dispersion coefficient (D) of silty clay was 1.4×10^{-4} m^2/d. The value of the retardation factor (R_d) was found to be 4.2–10. The results of the numerical simulation indicated that when the downstream was contaminated by Cr(Ⅵ), there was still a risk of pollution in the upstream even if molecular diffusion was not considered. The degree of pollution depended on the dispersity of the aquifer. Considering the adsorption of Cr(Ⅵ) by the aquifer, the higher the soil distribution coefficient, the smaller was the distribution range of the Cr(Ⅵ) pollution plume. Therefore, the transformation processes such as Cr(Ⅵ) adsorption should be focused on when predicting the distribution of Cr(Ⅵ) in contaminated sites.

Keywords: contaminated site; hexavalent chromium Cr(Ⅵ); migration and transformation; dispersion; numerical simulation

1 Introduction

With the increasing scale of global industrialization and the continuous advancement of urbanization, heavy metal pollution in soil and groundwater is becoming more and more serious[1–2]. Among them, the chromium pollution problem of groundwater due to the random piling of chromium slag and infiltration of chromium slag leachate is particularly prominent. Chromium (Cr) mainly exists in the form of +3 and +6 valence. Hexavalent chromium (hereinafter referred to as Cr(Ⅵ)) often exists in the environment as an ionic state[3], and it is 100– 500 times as toxic as trivalent chromium (hereinafter referred to as Cr(Ⅲ))[4–5]. Cr(Ⅵ) is carcinogenic, mutagenic and teratogenic[6]. China is the largest producer of the chromium chemical industry in the world. With the implementation of industrial structure adjustment, such as "retreating from the city to the park" and "shifting from a labor-intensive industry to service economy", a large number of chrome-contaminated sites have been left behind, and the remediation and treatment of chrome-contaminated sites are imminent. Therefore, it is of great significance to study the migra tion and transformation mechanism of Cr(Ⅵ) in soil–groundwater for the remediation of chromium-contaminated sites.

Many scholars studies on the temporal and spatial distribution, migration and transformation mechanism of chromium mainly focus on static adsorption test[7], soil-column test[8], box model test[9] and centrifuge test[10]. Zhang et al.[11] investigated the adsorption performance of Cr(Ⅵ) for the surface layer of Shanghai silty clay and the migration of Cr(Ⅵ) in surface soil under preferential flow conditions. The results showed that the adsorption of Cr(Ⅵ) by silty clay was consistent with Henry's isothermal adsorption, and the speed of heavy metal migration was related to the preferential flow and the amount of heavy metal adsorbed by clay via combining batch adsorption and soil-column tests. Zhao et al.[9] used a three-dimensional model sandbox to simulate the migration of Cr(Ⅵ) in the unsaturated zone and aquifer. Xu et al.[12] analyzed the effect of soil pH on the migration, morphological transformation and oxidation of Cr(Ⅲ). The above research reveals the migration and transformation of Cr(Ⅵ) in the soil–water medium under different conditions, but the migration parameters of Cr(Ⅵ) in the soil are not

Received: 08 August 2021 Revised: 01 December 2021
This work was supported by the National Key Research and Development Program of China (2019YFC1805905), the National Natural Science Foundation of China (42072318, 41972282, 41807253), the Opening Fund of the State Key Laboratory of Environmental Geochemistry (SKLEG2021208), the Natural Science Foundation of Hunan Province (2019JJ50763) and the Fundamental Research Funds for the Central Universities of Central South University (2021zzts0254).
First author: HE Yong, male, born in 1987, Doctor, Associate professor, doctoral supervisor, mainly engaged in research in environmental engineering geology and unsaturated soil mechanics. E-mail：heyong18@csu.edu.cn

obtained. In addition, the adsorption test generally adopts a small solid–liquid ratio, and the measured results are quite different from the soil-column test, which cannot accurately reflect the actual adsorption capacity of soil for pollutants[13]. Few studies have used the adsorption and soil-column tests for the comparative determination of Cr(Ⅵ) migration parameters in silty clay.

With the rapid development of computer technology, numerical simulation has become an important tool to study the migration and transformation of groundwater pollutants[14−18]. He et al.[19] used numerical simulation to study the migration of Cu^{2+} and Zn^{2+} and the blockage of bentonite engineering barrier in a tailings pond, and the results showed that after 5 years, the maximum migration distance of heavy metal ions reached 45 m, and the blocking efficiency of 0.5 m thick bentonite engineering barrier for pollutants exceeded 87%. LÜ et al.[20] established a two-dimensional numerical model of steady flow in the study area and determined the optimal location of permeable reaction walls in the contaminated site. At present, most of the existing studies use models to predict the migration dynamics and trend of chromium slag leachate[21−23], and rarely consider the migration and transformation of Cr(Ⅵ) in groundwater at the same time. The model parameters are mostly determined empirically and less often determined by experiments. In particular, there are few studies regarding the effect of pollution source location on the migration and distribution of Cr(Ⅵ) in groundwater.

In this paper, the chromium-contaminated site of a ferroalloy factory was taken as the study object. The distribution characteristics of soil and groundwater pollution were obtained through field investigation. Combined with adsorption, infiltration, and dispersion tests, the adsorption characteristics and migration patterns of Cr(Ⅵ) in silty clay samples were analyzed, and a three-dimensional dynamic model of Cr(Ⅵ) migration was established, considering convection, diffusion and adsorption. Visual MODFLOW was used to carry out three-dimensional visualization simulations of the Cr(Ⅵ) migration and transformation process in groundwater and to reveal the mechanism of Cr(Ⅵ) migration and transformation in the contaminated site.

2 Site investigation and laboratory experiment

2.1 Survey of the chromium-contaminated site

2.1.1 Overview of the chromium-contaminated site

The chromium-contaminated site selected in this paper is a ferroalloy smelter (as shown in Fig. 1). The factory was built in 1958, officially put into production in 1962, and it was completely eliminated in 2010. There was a wet smelting production line for chromium in the contaminated site. The long-term production and randomly piled chromium slag in the chromium slag yard resulted in severe Cr(Ⅵ) pollution in groundwater in the research area.

According to the geological drilling data of the chromium-contaminated site, the formation lithology in the study area is miscellaneous fill, silty clay, medium sand–silt, round gravel, and argillaceous siltstone from top to bottom. The miscellaneous fill contains perched water and receives recharge from atmospheric rainfall, surface runoff and factory drainage; the silty clay layer in the site is an aquiclude with poor permeability; the medium sand-silt layer, round gravel layer beneath the silty clay are the main confined aquifer, containing medium pore water, and receiving overflow recharge from atmospheric precipitation, artificial drainage and lateral runoff recharge from groundwater.

Fig. 1 Orientation diagram of the contaminated site

2.1.2 Survey of groundwater in the chromium-contaminated site

Based on the groundwater survey scheme, monitoring wells were arranged to collect groundwater samples, test the concentration of Cr(Ⅵ) in groundwater, and determine the pollution distribution characteristics of Cr(Ⅵ) in the site. In order to make the collected water samples representative, the monitoring wells were cleaned before sampling, and the groundwater samples were collected after backflow and stored promptly in a low-temperature incubator at 0–4℃ for testing. The detection method of water samples was in accordance with the requirements of *Standard for groundwater quality* (GB/T 14848-2017)[24], and the determination of Cr(Ⅵ) concentration was carried out according to the requirements of *Water quality-Determination of chromium (VI)-1,5 Diphenylcarbohydrazide spectrophotometric method* (GB/T 7467-1987)[25]. The coefficient of permeability of the confined aquifer was determined based on the field pumping test data.

2.2 Laboratory experiment

2.2.1 Experimental material

The soil samples used in the laboratory experiment were taken from the above-mentioned ferroalloy plant, and the sampling depth was 0–2 m. The basic physical and chemical properties of the in-situ soil samples were determined with reference to *Standard for geotechnical testing methods* (GB/T 50123-2019)[26], as shown in Table 1. According to the results of field survey, composition analysis and plasticity index results, it was determined that the soil sample used in this laboratory experiment was silty clay. X-ray fluorescence spectrometry (XRF) was used to determine the chemical composition of the soil sample, and the chemical composition of the soil sample was measured as follows: SiO_2 63.056%, Al_2O_3 19.483%, Fe_2O_3 11.048%, K_2O 1.979%, TiO_2

1.234%, SO_3 1.178%, MgO 0.873%, Cr_2O_3 0.315%, CaO 0.222%, Na_2O 0.200%, P_2O_5 0.119%, MnO 0.083%, ZnO 0.064%, and others 0.146%.

Table 1 Basic physicochemical properties of soil samples

Natural moisture content /%	Natural dry density /(g·cm^{-3})	Specific gravity	Plastic limit /%	Liquid limit /%	Plastic index	Total chromium content /(mg·kg^{-1})	Natural pH
24.97	1.56	2.61	22.4	37.3	14.9	439.6	4.93

Potassium dichromate ($K_2Cr_2O_7$) solution was used to simulate the groundwater of the chromium-contaminated site. In order to simulate the actual site conditions, the initial concentration of Cr(Ⅵ) contaminant in the infiltration and dispersion tests was set as 160 mg/L according to the site groundwater investigation results. The 2.83 g $K_2Cr_2O_7$ (pure analytical grade) was dissolved in a small amount of deionized water and then poured into a 1 L volumetric flask to prepare 1000 mg/L Cr(Ⅵ) mother liquor for later tests. The Cr(Ⅵ) solution used in adsorption, infiltration and dispersion tests were obtained by diluting the mother liquor, and the solution was re-prepared every 15 d.

2.2.2 Specimen preparation

After natural air drying, the soil samples were placed in an oven at 105℃ for 24 h. After cooling to room temperature, the samples were screened by a 0.5 mm sieve and stored in sealed plastic bags for the adsorption test.

The soil-column samples for the infiltration–dispersion test were prepared by static pressing. According to the target dry density (selected according to the density of the silty clay layer in the site), the natural air-dried soil samples with the corresponding mass and known moisture content were weighed and poured into the stainless steel sample ring of the infiltration–dispersion device (as shown in Fig. 2). The samples were pressed by the electronic universal testing machine with a displacement control method. The vertical loading rate was maintained at 0.2 mm/min, and the soil sample was uniformly compacted to the design position and stood for 1 h under a constant volume condition to prevent the sample from bouncing back. After unloading, a compacted sample with a diameter and height of 5 cm and an initial dry density of 1.5 ± 0.02 g/cm^3 was obtained.

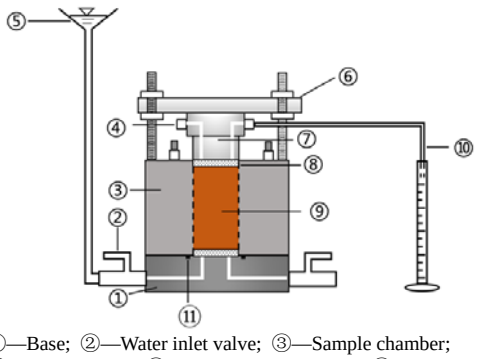

Note: ①—Base; ②—Water inlet valve; ③—Sample chamber; ④—Liquid outlet; ⑤—Constant head device; ⑥—Top cap; ⑦—Piston; ⑧—Porous stone; ⑨—Soil sample; ⑩—Pipette; ⑪—O ring.

Fig. 2 Schematic view of the permeability and dispersion device

2.2.3 Experimental equipment and method

(1) Adsorption test

The adsorption characteristics of Cr(Ⅵ) on silty clay surface at constant temperature were studied by batch adsorption test, and the model parameters such as distribution coefficient and retardation factor were measured. In order to accurately determine the actual adsorption capacity of silty clay on Cr(Ⅵ) , 9 samples of 25 g adsorbed soil were respectively placed in a 250 mL triangular flask. In the experiment, a comparatively large solid to liquid ratio of 1:4 recommended by Shackelford et al.[27] was adopted (referring to adding 4 mL Cr(Ⅵ) solution to 1 g soil sample), and the pH value was 5.6. The initial concentration of Cr(Ⅵ) increased from 10 mg/L to 1000 mg/L, and one group was distilled water control group. The triangular flasks containing the samples were numbered and oscillated in a 25℃ constant temperature oscillation box at 180 r/min for 24 h. After that, the supernatant was centrifuged for 10 min, and the concentration of Cr(Ⅵ) in the centrifuged supernatant was determined by the diphenylcarbohydrazide spectrophotometric method[25]. The adsorption capacity of soil on Cr(Ⅵ) q_e is

$$q_e = \frac{(C_0 - C_e)V}{m} \quad (1)$$

where C_0 is the initial concentration of Cr(Ⅵ) solution (mg/L); C_e is the concentration of Cr(Ⅵ) in centrifuged supernatant (mg/L); V is the volume of solution (L); and m is the soil mass (g).

(2) Infiltration and dispersion test

The infiltration–dispersion test apparatus was self-designed, as shown in Fig. 2. A saturated permeability test was carried out by the constant head method. When the coefficients of permeability calculated over adjacent long periods were constant, the permeability was considered to be stable, and the coefficient of permeability of the soil sample was calculated according to Eq. (2),

$$k = \frac{q}{Ai} = \frac{LV_t}{\Delta hAt} \quad (2)$$

where k is the coefficient of permeability (cm/s); q is the seepage flow (cm^3/s); i is the hydraulic gradient; A is the cross-sectional area of sample (cm^2); L is the height of sample (cm); V_t is the volume of solution flowing through the sample within t (cm^3); Δh is the hydraulic head difference (cm); and t is the time (s).

A Cr(Ⅵ) solution of 160 mg/L or 1 000 mg/L was introduced into distilled water after the completion of saturation and during the stable permeation. The coefficient of permeability of soil samples under the infiltration of Cr(Ⅵ) solution with different concentrations was determined. During the infiltration of Cr(Ⅵ) solution, the solution in the measuring cylinder was collected regularly, and the concentration of Cr(Ⅵ) in the effluent was determined by the diphenylcarbohydrazide spectrophotometric method. When the concentration of Cr(Ⅵ) in the effluent was close to that of the initial solution, the test was stopped. Combined with the

breakthrough curve model of pollutants proposed by Van Genuchten et al.[28], the parameter inversion method was adopted to determine the hydrodynamic dispersion coefficient and retardation factor of Cr(Ⅵ) in the sample. Meanwhile, based on the cumulative mass approach for column testing proposed by Shackelford[29], the retardation factor was calculated by the graphic method.

3 Numerical simulation

3.1 Simulation model

In this paper, the migration distribution characteristics of Cr(VI) in groundwater were simulated by the MODFLOW-2005 and MT3DMS modules in the numerical software Visual Modflow Flex 6.1. The model area was rectangular, 345.770 m long, 202.720 m wide, and 20.937 m deep. According to the stratigraphic distribution of the site, the model was vertically divided into five layers: (i) miscellaneous fill layer, (ii) silty clay layer, (iii) medium sand-silt-round gravel layer, (iv) strongly weathered mudstone and (v) moderately weathered mudstone, as shown in Fig. 3. Only the migration of pollutants in the saturated zone was considered in this study, hence the migration of Cr(Ⅵ) in the medium sand-silt-round gravel layer aquifer was simulated. With reference to the hydrogeological conditions of the research area, the constant head boundary conditions were given for the model. Since the aquifer had a certain embedment depth, the evaporation effect was neglected. Through field survey and head calibration, it was determined that the northwest boundary head was 51 m and the southeast boundary head was 50 m. Considering the rainfall infiltration recharge of the aquifer, the average annual rainfall in the study area was 2 483 mm, the rainfall infiltration recharge coefficient was 0.1, and the calculated rainfall infiltration recharge was 248.3 mm/a.

The shallow groundwater movement in the model region was simplified as a three-dimensional stable flow and described by the groundwater flow differential equation:

$$\frac{\partial}{\partial x}\left(k_x\frac{\partial h}{\partial x}\right)+\frac{\partial}{\partial y}\left(k_y\frac{\partial h}{\partial y}\right)+\frac{\partial}{\partial z}\left(k_z\frac{\partial h}{\partial z}\right)+q_s=S_s\frac{\partial h}{\partial t} \quad (3)$$

where h is the water level of the aquifer (m); k_x, k_y and k_z are the coefficients of permeability (m/s) in the x, y and z directions, respectively; q_s is the source/sink term (s^{-1}); and S_s is the water storage rate (m^{-1}).

Considering the convection, dispersion, adsorption of aquifer medium, and fluid source/sink term of groundwater in the study area, a convection–dispersion–adsorption three-dimensional solute migration partial differential equation was established to describe the migration of Cr(Ⅵ) in groundwater[14–15],

$$\theta R_d\frac{\partial C}{\partial t}=\frac{\partial}{\partial x_i}\left(\theta \boldsymbol{D}_{ij}\frac{\partial C}{\partial x_j}\right)-\frac{\partial}{\partial x_i}(q_iC)+ q_sC_s-\lambda_1\theta C-\lambda_2\rho_b\overline{C} \quad (4)$$

where θ is the porosity; R_d is the retardation factor; C is the dissolved concentration (g/m^3); $\boldsymbol{D}_{ij}$ is the tensor of hydrodynamic dispersion coefficient (m^2/s); q_i is the Darcy speed (m/s); C_s is the concentration of source/sink (g/m^3); λ_1 is the reaction rate constant of the dissolved phase (s^{-1}); λ_2 is the reaction rate constant of the adsorbed phase (s^{-1}); ρ_b is the bulk density of the porous medium (kg/m^3); and $\overline{C}$ is the adsorption concentration (mg/g), which is a function of the dissolved concentration C according to the adsorption isothermal relationship.

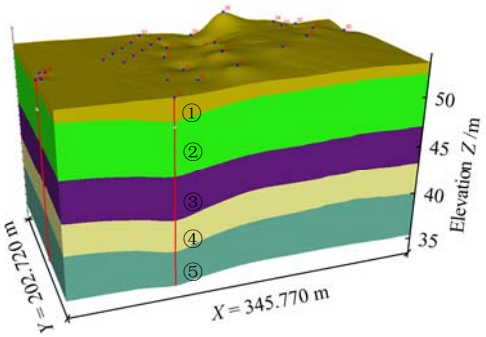

Note: ①—Miscellaneous fill; ②—Silty clay; ③—Medium sand-silt-round gravel; ④—Strongly weathered mudstone; ⑤—Moderately weathered mudstone.

Fig. 3 Three-dimensional stratigraphical structure model of the site

3.2 Model assumptions and parameters

It is assumed that the initial concentration of Cr(Ⅵ) in the model region was 0, and the pollution source was a 10 m×10 m regional source with a constant concentration of 120 mg/L. The pollution sources were set at the lower right corner (upstream), and upper left corner (downstream) of the model, and the site environment was assumed to be isothermal. At the same time, it is assumed that the stratigraphic medium in the same direction is uniform, and the molecular diffusion effect of Cr(Ⅵ) in the aquifer was not considered due to the large coefficient of permeability of the medium sand-silt-round gravel layer. The selection of model calculation parameters was mainly based on field experiments, laboratory experiments, research reports and literature[30–31].

Calculation parameters included the initial coefficient of permeability of the medium sand-silt-round gravel layer aquifer, aquifer characteristic parameters and pollutant migration parameters, and the specific values are shown in Table 2. The coefficient of permeability was determined through the single on-site single hole steady flow pumping test. The coefficients of permeability in the X and Y directions are the same, and the coefficient of permeability in the Z direction was 1/10 of the horizontal coefficient of permeability[32]. The bulk density was obtained by laboratory experiments, and other parameters were referred to the literature[30–31]. Based on the Visual MODFLOW PEST module, parameters were calibrated to obtain the groundwater seepage field and distribution after calibration. The ratio of transverse dispersity to longitudinal dispersity was 0.1, and the ratio of vertical dispersivity to longitudinal

dispersivity was 0.01[33–34].

Table 2 Parameters of medium sand-silt-round gravel aquifer used for calculation

Horizontal coefficient of permeability K_x /(m·s^{-1})	Water storage rate S_s /m^{-1}	Effective porosity θ_{Eff}	Total porosity θ_{Tot}	Longitudinal dispersity /m	Distribution coefficient K_d /(L·mg^{-1})	Bulk density ρ_b /(kg·m^{-3})
8.3×10^{-4}	1×10^{-4}	0.4	0.43	0, 13, 130	1.3×10^{-6}	2 000

4 Results and discussion

4.1 Survey of groundwater in the contaminated site

The testing results of confined pore water in the contaminated site are shown in Table 3.

Table 3 Statistics of analysis and testing results of confined groundwater

Test types	Screening criteria /(mg·L^{-1})	Total number of analysis	Number of over standard	Over standard rate /%	Maximum /(mg·L^{-1})	Minimum /(mg·L^{-1})	Mean /(mg·L^{-1})	Relative deviation /%
Cr(Ⅵ)	0.10	45	23	51.1	109	<0.01	21.20	30.60
As	0.05	44	NC	NC	NC	NC	NC	NC
Pb	0.10	44	0	0.0	0.02	<0.01	0.02	0.00
Mn	1.00	44	16	36.4	22.3	<0.01	2.11	3.98
Zn	5.00	44	0	0.0	0.96	<0.01	0.09	0.22

Note: NC indicates that it is lower than the laboratory detection limit and has not been calculated.

Among all the over standard indexes, Cr(Ⅵ) had the highest over standard rate of 51.1%, and the over standard multiple was up 1000 times. The next highest over standard rate was 36.4% for manganese, and the over standard multiple was as high as 22 times.

The field pumping test showed that the coefficient of permeability of the aquifer was 4.71×10^{-5}–8.3×10^{-4} m/s.

4.2 Migration and transformation test of hexavalent chromium

4.2.1 Batch adsorption test

Figure 4 shows the static equilibrium adsorption curve of Cr(Ⅵ) on the silty clay sample. With the increase of the initial concentration of Cr(Ⅵ), the amount of Cr(Ⅵ) available in the solution for soil adsorption increased, and the amount of Cr(Ⅵ) absorbed in the silty clay also increased rapidly and finally tended to equilibrium.

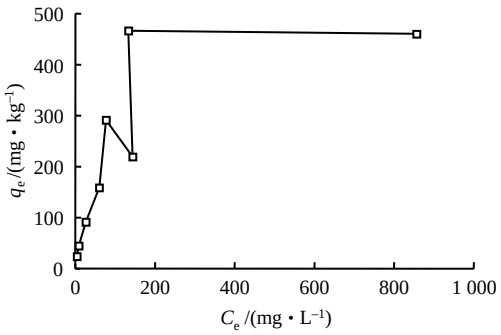

Fig. 4 Adsorption isotherm of silty clay for Cr(Ⅵ)

The Langmuir, Freundlich, D-R, and Henry models[35–36] were used to fit the adsorption isotherm, and the fitting parameters and the retardation factors calculated by each model are shown in Table 4. The correlation coefficient R^2 of the Langmuir model was 0.988 (as shown in Fig. 5), which was the closest to the experimental data. The adsorption capacity of the silty clay was 361.01 mg/kg.

Table 4 Adsorption isotherm parameters of Cr(Ⅵ) on silty clay

Adsorption model	Fitting equation	Parameter selection
Langmuir	$\frac{1}{q_e}=\frac{1}{\alpha\beta}\frac{1}{C_e}+\frac{1}{\beta}$, $R^2=0.988$	$\alpha=0.017$ L/mg $\beta=361.01$ mg/kg $R_d=1+\frac{\rho_b}{n}\frac{\alpha\beta}{(1+\alpha C)^2}=$ 1+21.661×(1+0.017 C)$^{-2}$
Freundlich	$q_e=K_F C_e^N$, $R^2=0.861$	$K_F=1.338\times10^{-5}$ L/mg $N=0.6$ $R_d=1+\frac{\rho_b}{n}K_F N C^{N-1}=$ 1+28.33 $C^{-0.4}$
D-R	$\ln(q_e)=\ln(q_m)-K\varepsilon^2$, $E=-\frac{1}{\sqrt{2K}}$, $R^2=0.913$	$K=0.007$ mol^2/kJ^2 $E=8.45$ kJ/mol
Henry	$q_e=K_d C_e$, $R^2=0.859$	$K_d=\frac{q_e}{C_e}=2.63\times10^{-6}$ L/mg $R_d=1+\frac{\rho_b}{n}K_d=10$

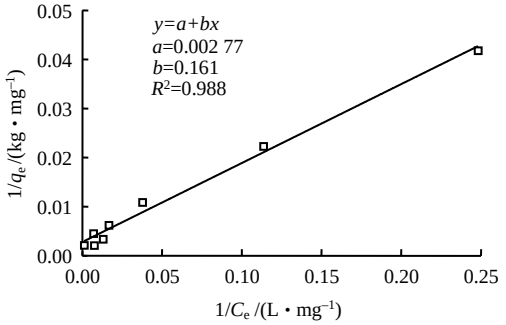

Fig. 5 Langmuir adsorption isotherm of silty clay for Cr(Ⅵ)

The constant of the Freundlich model was $N=0.6$, which was consistent with the study of Sharma et al.[37], indicating that the adsorption of the silty clay on Cr(Ⅵ) in within the initial concentration range selected in this paper was nonlinear. The maximum adsorption capacity (q_m) calculated by the D-R model was 1320.8 mg/kg, which was about 4 times the adsorption capacity calculated by the Langmuir model. This was because the D-R isothermal adsorption model was based on the assumption that the adsorbate was completely filled in the pores of the adsorbent. According to the calculation results of the D-R model, the equilibrium adsorption free energy was 8.45 kJ/mol, indicating that the adsorption mechanism of silty clay for Cr(Ⅵ) was ion exchange[38–39].

By comparing the above four static equilibrium adsorption models, it could be found that the adsorption of Cr(Ⅵ) by silty clay was more in line with the Langmuir model, and the maximum adsorption capacity calculated by the Langmuir model was the closest to the test results. Among them, the equilibrium adsorption free energy

of the D-R model could explain the adsorption mechanism of Cr(Ⅵ) by silty clay. In addition, the fitting results showed that when the equilibrium concentration of the solution was less than 200 mg/L, the adsorption of Cr(Ⅵ) by silty clay conformed to Henry's linear adsorption, and the adsorption distribution coefficient $K_d = 2.63\times10^{-6}$ L/mg and the retardation factor $R_d = 10$ were calculated according to the linear adsorption model. When the initial solution concentration was 160 mg/L, combined with the calculation formula in Table 4, the retardation factors calculated by the Langmuir and Freundlich models were 4.2 and 5.6, respectively.

4.2.2 Infiltration–dispersion test

The variation of the coefficient of permeability of soil samples under the infiltration of distilled water and Cr(Ⅵ) solution with different concentrations is shown in Fig. 6. From the figure, the coefficients of permeability of soil samples under the infiltration of distilled water and 160 mg/L Cr(Ⅵ) solution were close to each other, ranging from 6.5×10^{-7}–6.7×10^{-7} cm/s. When the concentration of Cr(Ⅵ) solution increased to 1 000 mg/L, the coefficient of permeability of the soil sample increased to 4.4×10^{-6} cm/s, indicating that the coefficient of permeability of silty clay increased under the effect of high concentration chemical solution. This might be because, under the effect of high concentration Cr(Ⅵ), the thickness of the diffusion electric double layer on the surface of clay mineral particles became thinner, and the effective porosity increased[40].

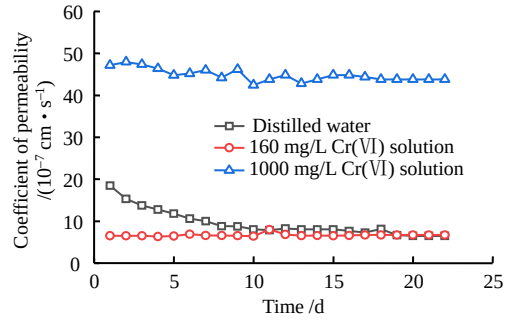

(a) Variation of coefficient of permeability with time

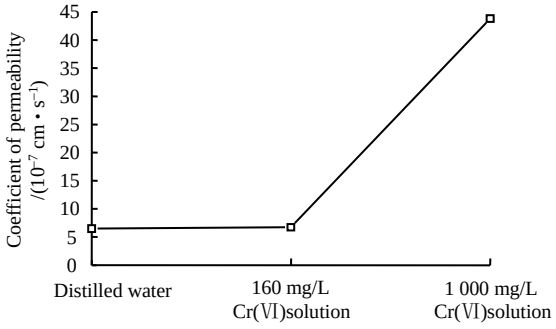

(b) Relationship between coefficient of permeability and concentration

Fig. 6 Variation of coefficient of permeability of silty clay under different solution infiltration

The breakthrough curve of Cr (Ⅵ) in silty clay is plotted in Fig. 7. The breakthrough curve of Cr(Ⅵ) in the soil sample is S-shaped, and the change of Cr(Ⅵ) concentration in effluent with time could be divided into three stages. Stage 1: when $t \leqslant 166$ h, Cr(Ⅵ) was not detected in the effluent. Before the dispersion test, the pores of the soil sample were saturated with distilled water. After 160 mg/L Cr(Ⅵ) solution was introduced, the effluent was displaced by distilled water. Therefore, the concentration of Cr(Ⅵ) in the effluent at the initial stage of the test was 0. However, the accumulative outflow volume of the solution in the first stage was 5.46 pore volumes (as shown in Fig. 8), indicating that with the infiltration of the solution, Cr(Ⅵ) was adsorbed and retained in the pores by the soil sample or undergone chemical interactions such as dissolution precipitation and redox with the soil, resulting in that Cr(Ⅵ) was detected in the outflow after 166 h. Stage 2: when $166\ \text{h} < t \leqslant 552$ h, Cr(Ⅵ) in the soil column reached a certain lower limit of accumulation concentration, and Cr(Ⅵ) began to flow out gradually. With the increase of Cr(Ⅵ) accumulation concentration in the soil column, the concentration of Cr(Ⅵ) in the effluent increased rapidly. Stage 3: when $t > 552$ h, the concentration of Cr(Ⅵ) in the effluent was close to the initial concentration of Cr(Ⅵ) solution, the adsorption of Cr(Ⅵ) by the soil sample basically reached saturation, the accumulation concentration of Cr(Ⅵ) in the soil column reached the upper limit, and the concentration of Cr(Ⅵ) in the effluent generally stopped changing.

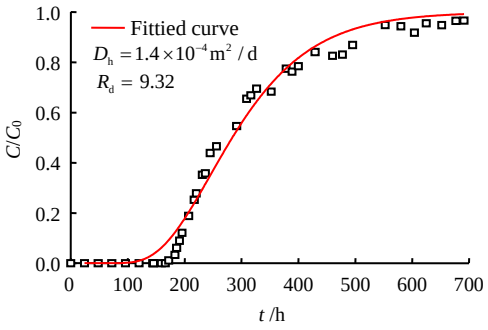

Fig. 7 Breakthrough curve of Cr(Ⅵ) in silty clay sample

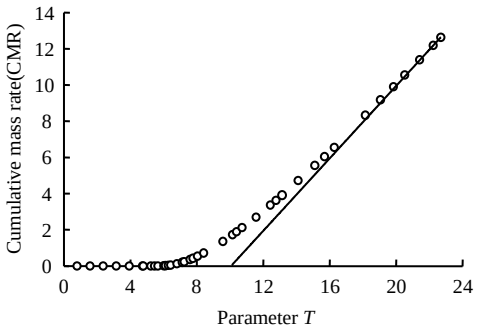

Fig. 8 Cumulative mass curve of Cr(Ⅵ) in silty clay

The hydrodynamic dispersion coefficient of Cr(Ⅵ) in the soil sample obtained by the parameter inversion method was 1.4×10^{-4} m^2/d, which was in good agreement with the available literature results[23]. However, the retardation factor of soil on Cr(Ⅵ) obtained by the parameter inversion method was 9.32, which was quite different from the retardation factor calculated by the

Langmuir and Freundlich models in the adsorption test (4.2 and 5.6, respectively). In order to further explore the influence of different calculation methods on the determination of pollutant migration parameters, the cumulative mass method was used to calculate the retardation factor and compared with the above results.

The cumulative mass curve of Cr(Ⅵ) in the soil sample is shown in Fig. 8, and the relevant calculation parameters are shown in Table 5. The retardation factor was calculated based on the relationship between the cumulative mass rate of Cr(Ⅵ) through the soil column and the parameter T in a certain time. The T value obtained by extending the straight-line part of Fig.8 to the X-axis was defined as T_0, $R_d = T_0$. As shown in Fig. 8, the test results in this paper were consistent with those described by Shackleford[29]. When $T > 8$, the cumulative mass rate basically increased in a positive proportional $R_d = T_0 = 10$. The retardation factor calculated by the cumulative mass method was the same as that calculated by Henry linear adsorption model in the adsorption test and was also consistent with the results obtained by the parameter inversion method, indicating that the larger solid-liquid ratio of 1:4 in the adsorption test in this paper was more consistent with the actual adsorption conditions of the soil.

Table 5 Parameters needed to calculate retardation factor by the cumulative mass method

C_0 /(mg·L^{-1})	Length of the sample /cm	Pore volume V_p /cm^3	Test time /h	Total fluid pore volume T	Average coefficient of permeability k /(cm·s^{-1})	Seepage velocity v /(cm·s^{-1})
160	5	41.70	352.35	11.57	6.46×10^{-7}	4.56×10^{-5}

4.3 Numerical simulation analysis

4.3.1 Hexavalent chromium migration in the contaminated site

Without considering the adsorption of Cr(Ⅵ) by the medium sand-silt-round gravel aquifer, a regional pollution source with an area of 10 m×10 m was set up at the upstream and downstream of the study area simultaneously (lower right corner and upper left corner of the model). The distribution of Cr(Ⅵ) pollution plume in groundwater after 30 and 730 d is shown in Fig. 9.

As can be seen from Figs. 9(a) and 9(b), Cr(Ⅵ) spread in a plume-like manner diffusion in the upstream and downstream regions. When the time increased from 30 d to 730 d, the distribution range of Cr(Ⅵ) pollution plume gradually increased. The difference was that under the influence of upstream pollution sources, the vertical distribution range of the pollution plume was large, and the tail color of the pollution plume was light. The farther the distance from the upstream pollution source, the lower the concentration of Cr(Ⅵ), and the concentration of Cr(Ⅵ) in groundwater had an obvious decaying trend with the increase of distance. When the pollution source was located downstream, the vertical distribution of the pollution plume was small and more concentrated. However, when the time increased from 30 d to 730 d, the pollution plume would expand from the downstream to the upstream; the concentration at the location of the pollution source remained at the initial concentration value of 120 mg/L input in the model (see the red pollution plume at the downstream in Fig. 9). Regardless of the distance from the downstream pollutant

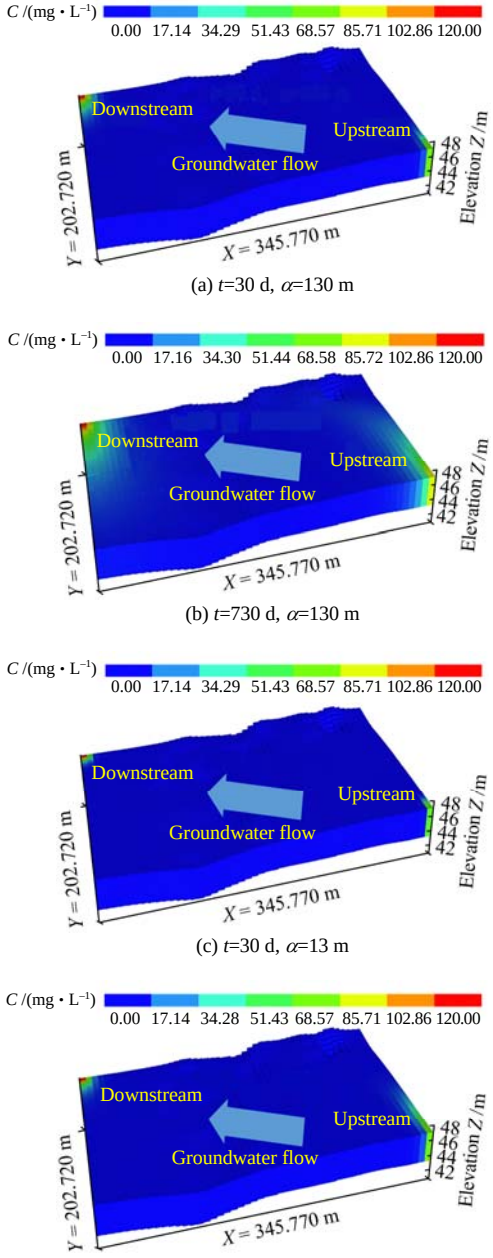

Fig. 9 Spatial and temporal distribution of Cr(Ⅵ) in aquifer when the pollution sources are located upstream and downstream

pollution source, the color of the pollution plume in the figure changed little, and the Cr(Ⅵ) concentration basically tended to be the same. The simulation results showed that even without considering the diffusion of Cr(Ⅵ) molecules, when the pollution source was located downstream of the site, the Cr(Ⅵ) pollution plume could still expand to the upstream area in a large area with the increase of time, and the Cr(Ⅵ) concentration in groundwater tended to be uniform. The decrease of concentration with increasing distance was not significant.

In fact, the migration mechanism of Cr(Ⅵ) in groundwater mainly included convection and dispersion. When the pollution source was located upstream of the site, Cr(Ⅵ) migrated from the upstream to the downstream with groundwater, and the process was mainly controlled by convection, with an extensive vertical distribution range of the pollution plume. At the same time, the pollutant concentration was fully diluted with the water flow, and the pollutant concentration gradually decreased with the increase of distance. When the pollution source was located downstream of the site, most pollutants migrated downstream with the water and did not enter the upstream area. However, due to the different pore paths and velocities of fluid particles in the aquifer medium, the water containing solutes moved at different speeds, the two water bodies would mix along the flow path, the solute concentration front expanded laterally and longitudinally simultaneously, and Cr(Ⅵ) produced mechanical dispersion in the aquifer. The dilution effect of water flow in this process was weak, coupled with the flat topography of the site (the northwest boundary head was 51 m, and the southeast boundary head was 50 m), the convection effect was weak and the distribution of Cr(Ⅵ) concentration in groundwater was more concentrated, and the pollutant concentration values were still at a high level farther away from the pollution source. This phenomenon was affected by the dispersity of aquifer, and the larger the dispersity of aquifer, the larger the area of the pollution plume extended from the downstream to the upstream by mechanical dispersion.

In order to verify the above process, the aquifer dispersity in the model was set to 13, and the other parameters remained unchanged. The simulation results are shown in Figs. 9(c) and 9(d). As can be seen from Fig. 9, when the pollution source was located upstream, the distribution pattern of Cr(Ⅵ) pollution plume was relatively consistent with the previous simulation results (as shown in Figs. 9(a) and 9(b)), and only the vertical distribution range was reduced, which is due to the smaller dispersity. When the pollution source was located downstream, after the dispersion was reduced by 10 times, the distribution range of the pollution plume was greatly reduced, indicating that the migration and distribution of the pollution plume were closely related to the dispersion of the aquifer. In order to prove that this conclusion was irrelative to the location of the pollution source set at the end of the calculation area, further numerical calculations were carried out considering only the effect of groundwater convection and without considering the mechanical dispersion of the aquifer (assuming that the dispersity was 0), and the obtained results are shown in Fig. 10. The results showed that Cr(Ⅵ) migrated downstream with the groundwater convection and moved forward in a piston flow with almost constant concentration without considering the effects of mechanical dispersion and molecular diffusion, under the action of upstream pollution sources. However, the Cr(Ⅵ) pollution plume located downstream no longer extended to the upstream when the dispersivity was 0. Compared with Figs. 9 and 10, it can be seen that the pollution plume did not expand in the opposite direction of groundwater flow when mechanical dispersion and molecular diffusion were not considered.

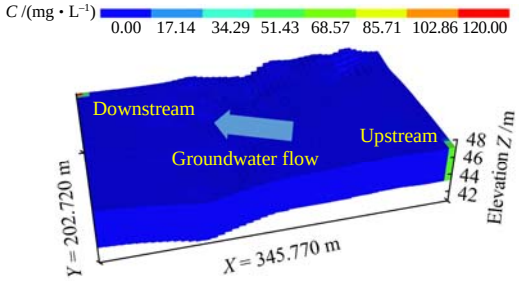

(a) t=30 d, α=0 m

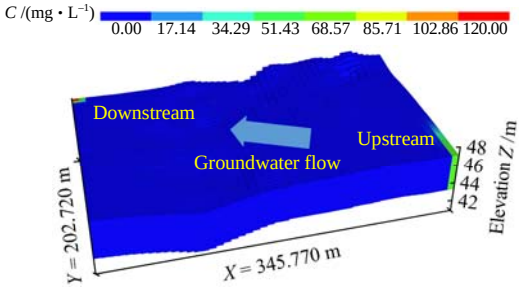

(b) t=730 d, α=0 m

Fig. 10 Spatial and temporal distribution of Cr(Ⅵ) in aquifer only considering convection

4.3.2 Hexavalent chromium migration considering adsorption

When the pollution source was set at upstream of the site. The contour of Cr(VI) mass concentration with considering adsorption and without considering adsorption is shown in Fig. 11.

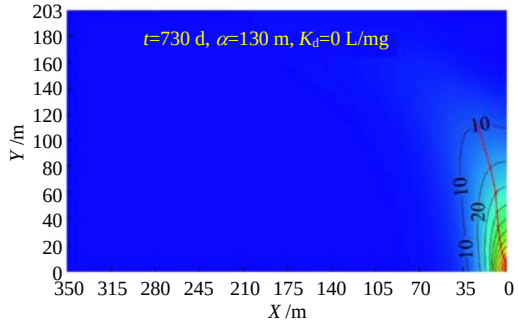

(a) Without considering adsorption

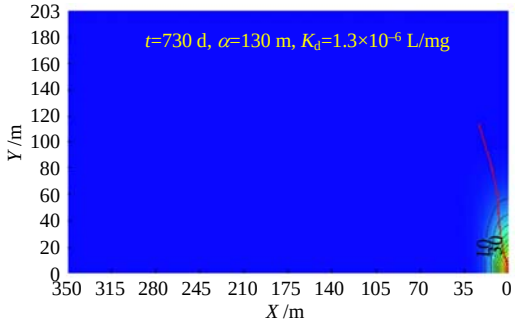

(b) Considering adsorption

Fig. 11 Mass concentration isolines of Cr(Ⅵ) without

considering adsorption and with considering adsorption

Figure 11 illustrates that under the same calculation parameters, regardless of the adsorption of Cr(Ⅵ) by aquifer media ($K_d = 0$ L/mg), the transverse diffusion distance of the pollution plume was 35 m, the longitudinal diffusion distance was 120 m, and the diffusion area was about 4200 m^2 after 730 d. Compared with Figs. 11(a) and 11(b), the adsorption of Cr(Ⅵ) by aquifer was regarded as linear isothermal adsorption ($K_d = 1.3\times 10^{-6}$ L/mg). After 730 d, the transverse diffusion distance of the pollution plume was 17 m, the longitudinal diffusion distance was 60 m, and the diffusion area was about 1020 m^2. In conclusion, considering adsorption, the diffusion range of Cr(Ⅵ) was reduced by 76%, and the distribution area of the high-concentration pollution plume is obviously reduced.

In order to further analyze the influence of adsorption on the temporal and spatial distribution of Cr(Ⅵ), several points were selected to form a line segment along the migration direction of the pollution plume (as shown in Fig. 11). The concentration distribution of Cr(Ⅵ) at each point on the line segment is shown in Fig. 12.

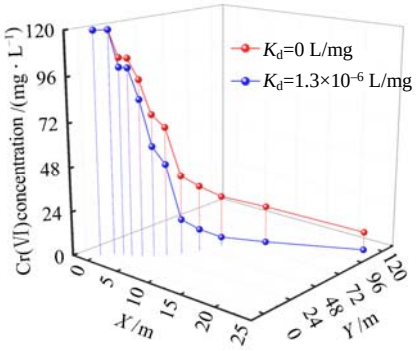

Fig. 12 Concentration distribution of Cr(Ⅵ) at different locations in the study area without considering adsorption and with considering adsorption (730 d)

When considering the adsorption of Cr(Ⅵ) by the aquifer medium, the concentration of Cr(Ⅵ) at each point was less than that at the same position without consider- ing the adsorption. As shown in Fig. 12, when Cr(Ⅵ) was diffused horizontally for 7 m and vertically for 35 m, the maximum difference of Cr(Ⅵ) concentration in the aquifer obtained by numerical calculation was 24 mg/L, which was about 20% of the initial concentration. The above study indicated that in addition to considering the convection–dispersion of pollutants when predicting the concentration distribution of Cr(Ⅵ) in groundwater, it was also necessary to focus on the adsorption of Cr(Ⅵ) by aquifer media and to determine the adsorption mode and adsorption parameters of Cr(Ⅵ) by aquifer media through laboratory experiments.

5 Conclusion

In this paper, the migration and transformation of Cr(Ⅵ) in silty clay and aquifer were studied by field survey, laboratory experiment and numerical simulation, and the main conclusions are as follows:

(1) The field survey showed that the groundwater in the chromium slag site of the ferroalloy plant in this study was mainly polluted by Cr(Ⅵ) and Mn(Ⅱ). Under the selected test conditions, the adsorption of Cr(Ⅵ) by silty clay conformed to the Langmuir isothermal adsorp- tion model, the maximum adsorption capacity was about 466.6 mg/kg, and the adsorption mechanism was ion exchange.

(2) Under the infiltration of low concentration Cr(Ⅵ) solution, the coefficient of permeability of silty clay sample did not change much; under the infiltration of high concentration Cr(Ⅵ) solution, the coefficient of permeability of silty clay sample increased. The hydro-dynamic dispersion coefficient and retardation factor were fitted by van Genuchten and Parker convection–dispersion analytical solutions. The fitted retardation factor was basically consistent with the retardation factor calculated by the cumulative mass method of soil column test and Henry adsorption model and was quite different from the Langmuir and Freundlich models.

(3) Even if the pollution source was located in the downstream area of the site, the pollution plume could still extend from the downstream to the upstream of the site through mechanical dispersion, resulting in upstream groundwater pollution. The degree of pollution depended on the dispersity of the aquifer.

(4) Considering the stratigraphic adsorption, the calculated pollutant concentration and pollution plume area were reduced, and the interaction between Cr(Ⅵ) and the site geotechnical medium should be considered in the formulation of groundwater pollution prevention and control and remediation schemes.

References

[1] CHEN Yun-min, SHI Jian-yong, ZHU Wei, et al. A review of geoenvironmental engineering[J]. China Civil Engineering Journal, 2012, 45(4): 165–182.

[2] FENG S J, PENG M Q, CHEN Z L, et al. Transient analytical solution for one-dimensional transport of organic contaminants through GM/GCL/SL composite liner[J]. Science of the Total Environment, 2019, 650: 479–492.

[3] ZHU F, LIU T, ZHANG Z, et al. Remediation of hexavalent chromium in column by green synthesized nanoscale zero-valent iron/nickel: factors, migration model and numerical simulation[J]. Ecotoxicology and Environmental Safety, 2021, 207: 111572.

[4] KANWAL F, REHMAN R, MAHMUD T, et al. Isothermal and thermodynamical modeling of chromium (III) adsorption by composites of polyaniline with rice husk and saw dust[J]. Journal of the Chilean Chemical Society, 2012, 57: 1058–1063.

[5] TOFAN L, PADURARU C, TEODOSIU C, et al. Fixed bed column study on the removal of chromium (III) ions

from aqueous solutions by using hemp fibers with improved sorption performance[J]. Cellulose Chemistry and Technology, 2015, 49: 219–229.

[6] SILVIO D F. Threshold mechanisms and site specificity in chromium (VI) carcinogenesis[J]. Carcinogenesis, 2000, 21: 533–541.

[7] ZHANG X, TONG J, HU B X, et al. Adsorption and desorption for dynamics transport of hexavalent chromium (Cr(Ⅵ)) in soil column[J]. Environmental Science and Pollution Research, 2018, 25: 459–468.

[8] FAN Ri-dong. Study on chemical compatibility and containment performance of soil-bentonite cutoff wall exposed to heavy metal contaminants[D]. Nanjing: Southeast University, 2017.

[9] ZHAO X, SOBECKY P A, ZHAO L, et al. Chromium (VI) transport and fate in unsaturated zone and aquifer: 3D sandbox results[J]. Journal of Hazardous Materials, 2016, 306(5): 203–209.

[10] ZHANG Jun-jie. Study on the migration law of hexavalent chromium in unsaturated zone through centrifugal test[D]. Chengdu: Chengdu University of Technology, 2018.

[11] ZHANG Wen-jie, JIAO Wei-guo, GENG Xiao, et al. Experimental investigation on migration of typical heavy metals under preferential flow[J]. Rock and Soil Mechanics, 2020, 41(Suppl.2): 1–7.

[12] XU T, NAN F, JIANG X F, et al. Effect of soil pH on the transport, fractionation, and oxidation of chromium (Ⅲ)[J]. Ecotoxicology and Environmental Safety, 2020, 195: 110459.

[13] WANG Yu-ze. Soils modification for liners and service life analysis[D]. Hangzhou: Zhejiang University, 2014.

[14] TIWARY R K, DHAKATE R, RAO V A, et al. Assessment and prediction of contaminant migration in groundwater from chromite waste dump[J]. Environmental Geology, 2005, 48(4): 420–429.

[15] ZHENG Chun-miao, BENNETT G D. Applied contaminant transport modeling[M]. Beijing: Higher Education Press, 2009.

[16] XIE Hai-jian, CHEN Yun-min, LOU Zhang-hua. An analytical solution to contaminant transport through composite liners with geomembrane defects[J]. Science China-Technological Sciences, 2010, 40(5): 486–495.

[17] MA Peng-fei, LI Shu-chen, WANG Xiu-wei, et al. Nonlocal peridynamic method for porous media seepage simulation[J]. Rock and Soil Mechanics, 2021, 42(11): 3147–3156.

[18] GOPINATH R, POOPATHI R, VASANTHAVIGAR M, et al. Stabilized red soil—an efficient liner system for landfills containing hazardous materials[J]. Environmental Monitoring and Assessment, 2018, 190 (10): 590.

[19] HE Y, LI B B, ZHANG K N, et al. Experimental and numerical study on heavy metal contaminant migration and retention behavior of engineered barrier in tailings pond[J]. Environmental Pollution, 2019, 252: 1010–1018.

[20] LÜ Yong-gao, CAI Wu-tian, YANG Li, et al. A numerical simulation study of the position optimization of a pilot-scale permeable reactive barrier: a case study of the hexavalent chromium contaminated site[J]. Hydrogeology and Engineering Geology, 2020, 47(5): 189–195.

[21] KHAN A A, MUTHUKRISHNAN M, GUHA B K. Sorption and transport modeling of hexavalent chromium on soil media[J]. Journal of Hazardous Materials, 2010, 174: 444–454.

[22] HARWOOD J A. Investigation of fate and migration of hexavalent chromium at the mouat industries site, columbus, montana[D]. Montana: Montana Tech, 2016.

[23] LIU Ling, XIAO Li-ping, LI Xi-lin. Simulation of migration of hexavalent chromium in groundwater[J]. Journal of System Simulation, 2018, 30(2): 560–568.

[24] Ministry of Water Resources of the People's Republic of China. GB/T 14848－2017 Standard for groundwater quality[S]. Beijing: Standards Press of China, 2017.

[25] Ministry of Ecology and Environment of the People's Republic of China. GB/T 7467－1987 Water quality-determination of chromium (Ⅵ)-1, 5-diphenylcarbohydrazide spectrophotometric methods [S]. Beijing: Standards Press of China, 1987.

[26] Ministry of Housing and Urban-Rural Development of the People's Republic of China. GB/T 50123－2019 Standard for geotechnical testing method[S]. Beijing: China Planning Press, 2019.

[27] SHACKELFORD C D, REDMOND P L. Solute breakthrough curves for processed kaolin at low flow rates[J]. Journal of Geotechnical Engineering, 1995, 121(1): 17–32.

[28] VAN GENUCHTEN M T, PARKER J C. Boundary conditions for displacement experiments through short laboratory soil columns[J]. Soil Science Society of America Journal, 1984, 48(4): 703–708.

[29] SHACKELFORD C D. Cumulative mass approach for column testing[J]. Journal of Geotechnical Engineering, 1995, 121(10): 696–703.

[30] Ministry of Ecology and Environment of the People's Republic of China. Guidelines for the assessment of groundwater pollution simulation and prediction[R]. Beijing: Ministry of Ecology and Environment, 2019.

[31] Hunan HIKEE Environmental Technology Co., Ltd. Detailed geotechnical investigation report of a contaminated site[R]. Changsha: Hunan HIKEE Environmental Technology Co., Ltd., 2021.

[32] CHEN Yong-gui, HE Yong, ZHOU Xing-zhi. Retention

of heavy metal ion on engineering barriers of compacted bentonite[J]. Journal of Central South University (Science and Technology), 2012, 43(10): 4038–4043.

[33] YENIGÜL N B, ELFEKI A M M, GEHRELS J. Reliability assessment of groundwater monitoring networks at landfill sites[J]. Journal of Hydrology, 2005, 308(1–4): 1–17.

[34] SIECZK A A, BUJAKOWSKI F, FALKOWSKI T, et al. Morphogenesis of a floodplain as a criterion for assessing the susceptibility to water pollution in an agriculturally rich valley of a lowland river[J]. Water, 2018, 10(4): 399.

[35] LI Zhen-ze. Mechanism of sorption, desorption, diffusion and remediation of heavy metals in soils[D]. Hangzhou: Zhejiang University, 2009.

[36] CHEN Yun-min, WANG Yu-ze, XIE Hai-jian, et al. Adsorption characteristics of loess-modified natural silt towards Pb (II): equilibrium and kinetic tests[J]. Chinese Journal of Geotechnical Engineering, 2014, 36(7): 1185–1194.

[37] SHARMA H D, REDDY K R. Geoenvironmental engineering: site remediation, waste containment, and emerging waste management technologies[M]. New Jersey: Wiley, 2004.

[38] VIJAYARGHAVAN K, PADMESH T V, PALANIVELU K, et al. Biosorption of nickel (II) ions onto Sargassum wightii: application of two-parameter and three-parameter isotherm models[J]. Journal of Hazardous Materials, 2006, 133(1/3): 304–308.

[39] DO D D. Adsorption analysis: equilibrium and kinetics[M]. London: Imperial College Press, 1998.

[40] HE Y, WANG M M, WU D Y, et al. Effects of chemical solutions on the hydromechanical behavior of a laterite/bentonite mixture used as an engineered barrier[J]. Bulletin of Engineering Geology and the Environment, 2020, 80(3): 1–12.